

Biomimetic surfaces with patterned wettability for high-efficiency dehumidification and fog harvesting

Xinhui Song^{1,*,+}, Qijia Zhou^{2,+}, Bochao Cai^{3,&}, Ziyi Qiu^{4,&}

¹School of Environmental and Material Engineering, Yantai University, Yantai, 264005, China

²Department of Chemistry and Biochemistry, University of California Santa Cruz, California, 95064, United States

³Wuhan Haidian Foreign Language Shiyuan School, Wuhan, 430223, China

⁴Shanghai Foreign Language Academy, Shanghai, 200233, China

* Songxinhuijn22@163.com

+These authors contributed equally to this work and should be considered co-first authors.

&These authors contributed equally to this work and should be considered co-second authors.

Abstract. In this paper, by studying the characteristics of the bionic surface with pattern wettability, the process of its efficient dehumidification and atomization is explored. This paper briefly introduces the importance of dehumidification and physicochemical and the market demand, and also introduces the properties of superhydrophobic materials. The theoretical part mainly describes the basic principle of superhydrophobicity and the Wenzel and Cassie-Baxter models. Subsequently, natural and synthetic superhydrophobic surfaces are introduced, involving Namib beetles, butterfly wings, and so on. The final article points out that superhydrophobic surfaces can be used in numerous fields, especially in fog collection. However, the improvement of durability is the focus of attention for superhydrophobic surfaces. In future research, attention needs to be paid to the use of materials and the efficiency of fog collection.

Keywords: dehumidification, superhydrophobic surface, fog harvesting, application.

1. Introduction

1.1. Need for dehumidification and Fog harvesting

Dehumidification is the process of removing vapor from the atmosphere. The process can be achieved by increasing the pressure or cooling the air. It is also valid to use liquid or solid to adsorb the vapor, which is called a desiccant. This technique is widely used in our daily life, such as keeping the food dry in a sealed container. Dehumidification can be used to harvest fog. For example, some desert areas only have 10 inches of rain per year, and some cities are also suffering from a lack of water. To overcome the shortage of water, fog harvesting can be a significant source of water for arid regions. Both dehumidification and fog harvesting are critical techniques to deal with various situations.

1.2. Market size / impact / energy consumption

It is reported that the global market size for dehumidification in 2020 was around 3.5 billion U.S. dollars, and the demand for dehumidification is expected to keep increasing. Experts predict that the annual growth rate is going to be about 7.0% from 2021 to 2028 [1]. Dehumidification is irreplaceable. It can not only help improve the living environment to prevent the growth of mold but also provide a more ideal environment for some experiments to control the reaction condition. Some people argue that air conditioners can take place of dehumidifiers since air conditioners also have a dehumidification mode. However, compared with dehumidifiers, the effect of air conditioners' dehumidification is unsatisfactory. To be specific, in order to dehumidify, air conditioners will blow cold air which makes people uncomfortable. Also, air conditioners can only be utilized under limited conditions. For example, it is not suitable to install an air conditioner in the bathroom or kitchen. Furthermore, air conditioners' dehumidification mode will cause abundant power consumption, which will increase the load of operation and lead to a shortening of the service life. In contrast, dehumidifiers not only have high working efficiency but also have a better dehumidification effect than air conditioners. The working principle of dehumidifiers is drawing moist air into the machine by a fan and passing it through a heat exchanger. Then, the vapor in the moist air will condense into water droplets, and the dry air will discharge from the machine to reduce indoor humidity.

From the perspective of energy consumption, dehumidifiers are environmentally friendly. An average small 30-pint dehumidifier uses 300W of energy, while an average big 70-pint dehumidifier uses 700W of energy. In comparison, an air conditioner uses 3300W of energy [2]. Dehumidifier only costs between \$0.03 to \$0.16 per hour and \$0.72 to \$3.84 per day [3]. After all, dehumidifiers have a better impact than air conditioners.

1.3. Definitions and applications of superhydrophobic surfaces

Superhydrophobic surfaces are surfaces that can readily repel water droplets. When a water droplet is placed on a superhydrophobic surface, the contact angle (θ) will be $150^\circ < \theta < 180^\circ$, and the water droplet will also display low hysteresis. Usually, it's hard for a superhydrophobic surface to form a bond with the water molecules, thus a water droplet can easily slide down and not adhere to its surface. The applications of superhydrophobic surfaces are broad. For instance, superhydrophobic surfaces can reduce liquid adhesion to manufacturing equipment and improve the condensation process. Superhydrophobic surfaces are also applied in our daily design. For example, they are applied to tents and camping gear. Plus, superhydrophobic surfaces exist in insects and plants organism as well. Water striders' superhydrophobic feet enable them to stand and walk on water.

1.4. Properties of superhydrophobic materials

Materials that are superhydrophobic often have low surface energies. A solid surface's surface energy is directly correlated with how hydrophobic it is. A hydrophobic solid has a contact angle with water that is larger than 90 degrees. Among the materials that are known to be hydrophobic, organosilicon and organofluoride compounds have low surface energies, and the surface energies of fluorinated groups decline in the following order: $-\text{CH}_2 > -\text{CH}_3 > -\text{CF}_2 > -\text{CF}_2\text{H} > -\text{CF}_3$. Where $-\text{CF}_3$ has a maximum water contact angle of 120 degrees and surface energy as low as 6.7 mJ/m^2 . Both a solid surface's chemical make-up and microstructure affect how moist it is overall.

1.5. Scope of the article

In this article, surface tension, surface energy, contact angle, contact angle hysteresis, wetting states, surface geometry effects, surfaces with patterned wettability, filmwise, and dropwise condensation are reviewed. Then, the natural surfaces of the Namib desert beetle's wings, butterfly wings, and spider webs are introduced. The corresponding utility of different biomimetic surfaces with patterned wettability is also explained. Finally, the limitations of the technologies are discussed.

2. Theory

2.1. Surface tension and surface energy

Surface tension is a term used to describe the attraction between molecules in a liquid. The direction of surface tension is perpendicular to the border separating any two liquid level portions and tangent to the liquid level. There is a wide variety of surface tension in different liquids, and its value falls somewhat as the temperature rises. While a liquid with a high surface tension will have a bigger contact angle, one with low surface energy will have a smaller contact angle (see Figure 1). Additionally, contaminants can make a liquid's surface tension less stable. For instance, the surface tension of clean water (72.1 mN/m at 25 °C) is high, but when soap is added to the water, the surface tension drops.

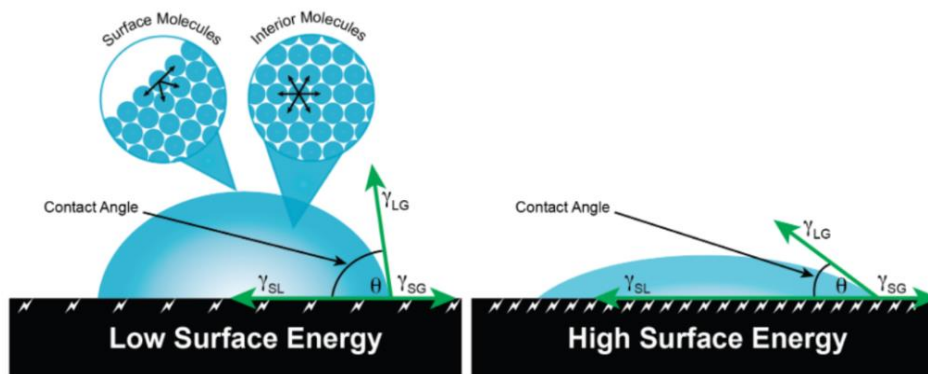


Figure 1. The relationship between surface tension and contact angle. [4].

Surface energy γ_{sv} is the nonvolumetric work needed for the material to increase the surface area reversibly under the condition of constant temperature, constant pressure, and constant composition. In other words, surface energy is the extra energy of a surface particle relative to an interior particle. Surface energy is a measure of the breakdown of chemical bonds between molecules to create a new surface in the material.

2.2. Contact angle, contact angle hysteresis

The angle between the solid-liquid interface and the gas-liquid interface at the intersection of solid, liquid, and gas is referred to as the contact angle (see Figure 2). A hydrophilic solid surface may be easily moistened by water if the contact angle is less than 90 degrees. The wettability increases with decreasing contact angle. The solid surface is hydrophobic, on the other hand, and does not readily absorb water if the contact angle is larger than 90°. The Young's equation gives the contact angle for a liquid on a flat surface:

$$\cos \theta = \frac{\gamma_{sv} - \gamma_{sl}}{\gamma_{lv}} \quad (1)$$

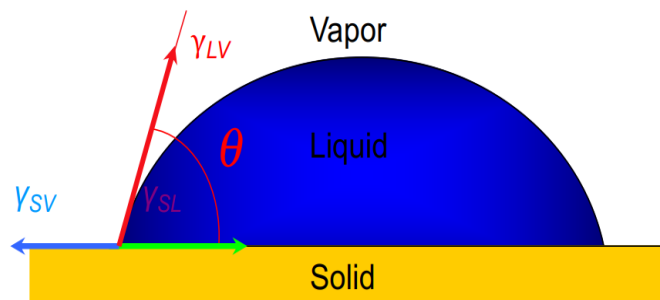


Figure 2. The diagram of the contact angle of a liquid droplet.

The activation energy needed to shift a droplet from one metastable state to another on a surface is reflected in contact angle hysteresis [5]. The difference between advancing and retreating contact angles is referred to as hysteresis (see Figure 3).

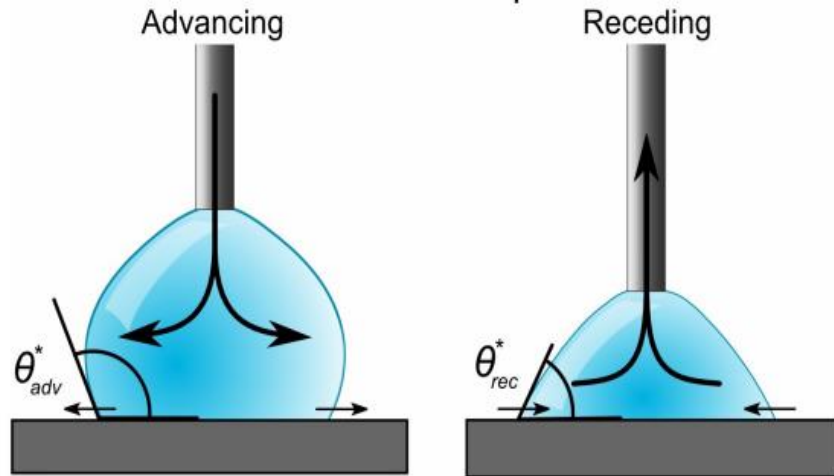


Figure 3. Advancing and receding contact angle of a sessile drop.

Wetted roughness, chemical heterogeneity, and condensation next to the drop all contribute to the difference between advancing and retreating contact angles. The contact angle is known as the advancing contact angle as a sessile droplet enlarges. The contact angle between a retreating droplet and a solid is referred to as the receding contact angle. Additionally, sliding drops can use advancing and receding contact angles (see Figure 4).

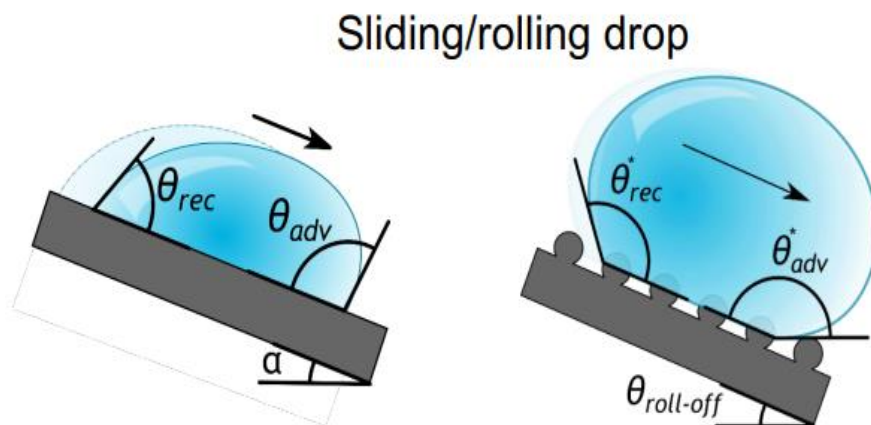


Figure 4. Advancing and receding contact angle of a sliding drop.

The lower the difference between advancing and receding contact angle, the easier it is for the droplet to slide down. The sliding angle for a droplet can be related to the advancing and receding contact angles through the Furmidge relationship, given as

$$\sin \alpha = \frac{w\gamma_{LV}}{mg} (\cos \theta_{rec} - \cos \theta_{adv}) \quad (2)$$

where α is the sliding angle and w is the width of the droplet. Overall, hysteresis affects how readily a droplet can slide down a surface.

2.3. Wenzel state and Cassie-Baxter state

In real life, most surfaces are textured, rather than smooth and flat. On a rough surface, a contacting liquid can form either the Wenzel state or the Cassie-Baxter state. Instead of simply applying Young's equation, surface roughness needs to be taken into account. The surface roughness factor R_f is defined as

$$R_f = \frac{A_{SL}}{A_F} \quad (3)$$

where $R_f > 1$, A_{SL} is the rough surface area, and A_F is the flat projected area. By increasing the roughness, both hydrophilicity and hydrophobicity will be increased. In Wenzel state, liquid can fill into the surface texture (see Figure 5).

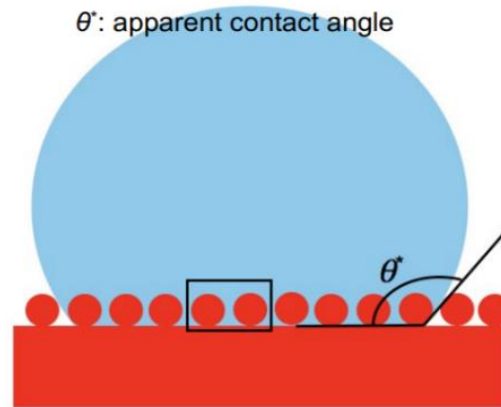


Figure 5. The Wenzel State.

Based on the force balance and empirical considerations, the Wenzel equation is determined as

$$\cos \theta = \frac{dA_{LA}}{dA_F} = \frac{A_{SL}}{A_F} \frac{dA_{LA}}{dA_{SL}} = R_f \cos \theta^* \quad (4)$$

where θ^* is the apparent contact angle, and θ is the young's angle (real contact angle).

The situation above is called the homogeneous interface. However, when a liquid droplet on a rough surface forms a heterogeneous interface, it will lead to the Cassie-Baxter state. Homogeneous means the only thing filling the surface texture is the contacting liquid, while heterogeneous means that both the contacting liquid and air are filling in the texture. The liquid can only partially fill the roughness of the surface (see Figure 6).

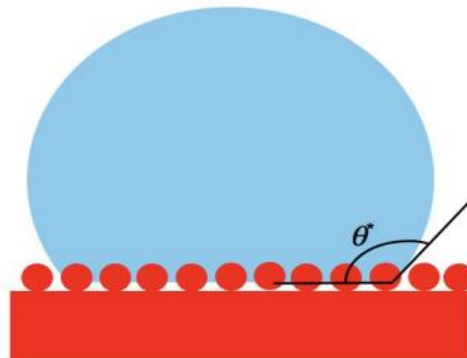


Figure 6. The Cassie-Baxter State.

The Cassie equation yields the contact angle at a heterogeneous interface, which consists of two fractions:

$$\cos \theta = f_1 \cos \theta_1 + f_2 \cos \theta_2 \quad (5)$$

where f_1 , f_2 are the fractional areas, and $f_1 + f_2 = 1$. Since a composite interface (see Figure 7) consists of a fractional geometrical area of the solid-liquid interface ($f_1 = f_{SL}, \theta_1 = \theta$) and the liquid-air interface ($f_2 = f_{LA} = 1 - f_{SL}, \cos \theta_2 = -1$).

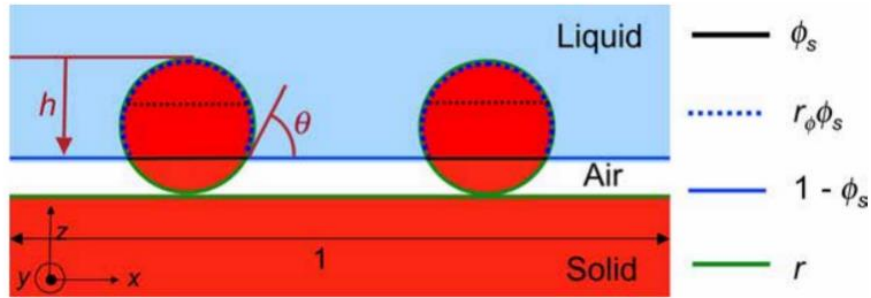


Figure 7. The diagram of a composite interface.

By combining equation (3) and equation (5), the Cassie-Baxter equation will be obtained

$$\cos \theta^* = r_\phi \phi_s \cos \theta + \phi_s - 1 \quad (6)$$

where r_ϕ is the roughness of the solid surface, ϕ_s is the fraction of the solid surface, and $r_\phi \phi_s = R_f f_{SL}$.

In conclusion, the Cassie-Baxter state is preferable for creating non-wetting fields, whereas the Wenzel state is favored for creating wetting surfaces. The Wenzel state will have large apparent contact angles and strong contact angle hysteresis if is more than 90° . It will have low visible contact angles and strong inertia if is below 90° . The Cassie-Baxter condition, on the other hand, will often result in high seeming contact angles and minimal surface morphology hysteresis, independently of whether is bigger or less than 90° .

2.4. Effects of surface geometry

Surface geometry also determines the wetting state. To support a composite interface, the liquid must meet its equilibrium contact angle locally. If $\theta \geq \Psi$, where Ψ is the texture angle (see Figure 8), then it will lead to a Cassie-Baxter state and the liquid doesn't permeate into the texture.

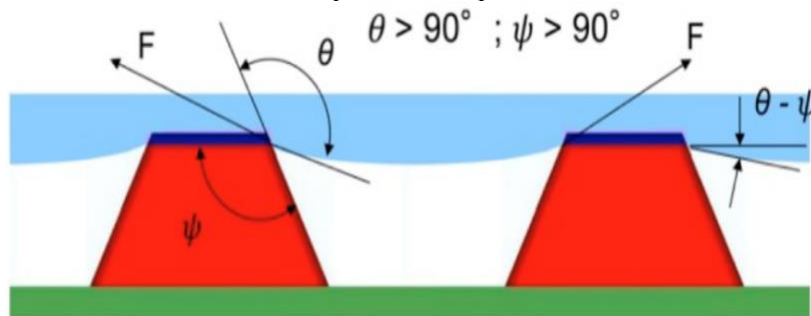


Figure 8. The composite interface.

On the other hand, if $\theta < \Psi$ (see Figure 9), then it will lead to a Wenzel state and the liquid will be imbibed into the surface texture, because the Young's condition is not satisfied.

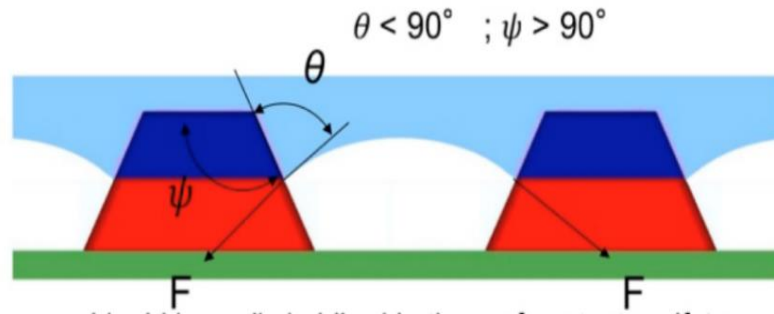


Figure 9. The wetted interface.

The situations above are discussed under the condition of the texture angle $\Psi > 90^\circ$. However, if the texture angle $\Psi < 90^\circ$, then the surface texture is called re-entrant texture (see Figure 10). Under the re-entrant texture premise, if $\theta > \Psi$, it will always lead to Cassie-Baxter state since the liquid doesn't permeate the texture. Such a surface can support a composite interface even if $\theta < 90^\circ$.

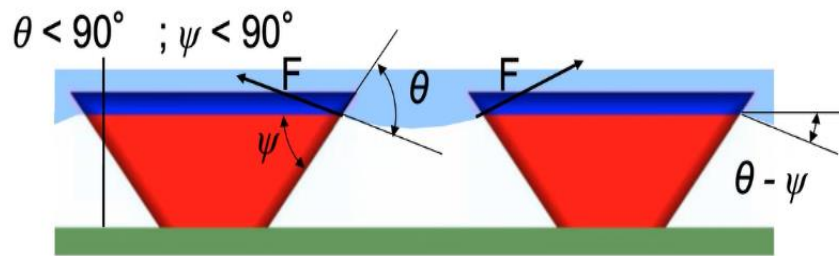


Figure 10. The re-entrant texture.

Based on the texture features above, it can be concluded that the ideal superhydrophobic interfaces should have the texture angle Ψ smaller than the Young's contact angle θ [6]. When $\Psi > 90^\circ$, it is hard for the texture to repel low surface tension liquids such as different oils or alcohols, but it may still be able to repel water droplets.

2.5. Surfaces with patterned wettability

Water harvesting is frequently accomplished by using surfaces with patterned wettability. The Namib desert beetles, for instance, have a special manner of obtaining water in the dry desert. They have superhydrophilic riblet veins and superhydrophobic riblet grooves on their wings. They can gather fog droplets in the wind by combining their superhydrophilicity and superhydrophobicity. The hydrophilic parts first gather the water droplets. The water droplet expands as it rolls down the back of the bow and into the desert beetle's mouth.

Based on the fog harvesting technique of the desert beetles, a star-shaped moisture pattern has been designed. It turns out that star surfaces have a greater efficiency by integrating wettability and shape gradient. It turns out that star surfaces (see Figure 11) have higher efficiency in water harvesting than circular or uniform wettability patterns.

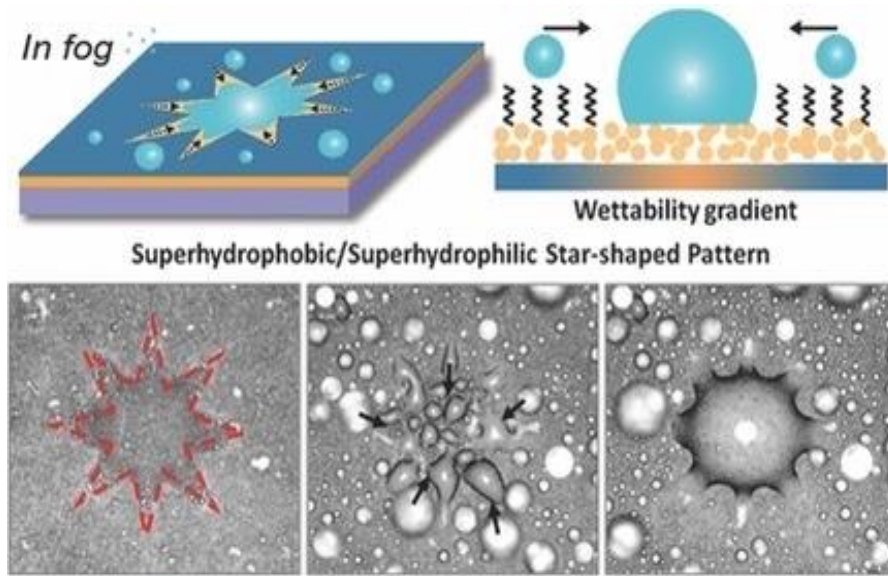


Figure 11. The Star-shaped pattern [7].

TiO₂ fluid was spin-coated over a naked glass substrate to produce a superhydrophilic surface with a starry fluid flow pattern (see Figure 12a). Using heptadecafluorodecyl-trimethoxysilane (FAS), the film's wettability was then altered from superhydrophilic to superhydrophobic (see Figure 12b). The photocatalytic breakdown of the FAS monolayer caused the FAS-modified superhydrophobic TiO₂ surface to become back to superhydrophilic (see Figure 13), which was accomplished by utilizing photomasks with circular pattern patterns or 4-, 5-, 6-, and 8-pointed star-shaped patterns. On surfaces having star-shaped wettability patterns, fog droplets might be deliberately collected in the direction of more hygroscopic areas (see Figure 12c) [7].

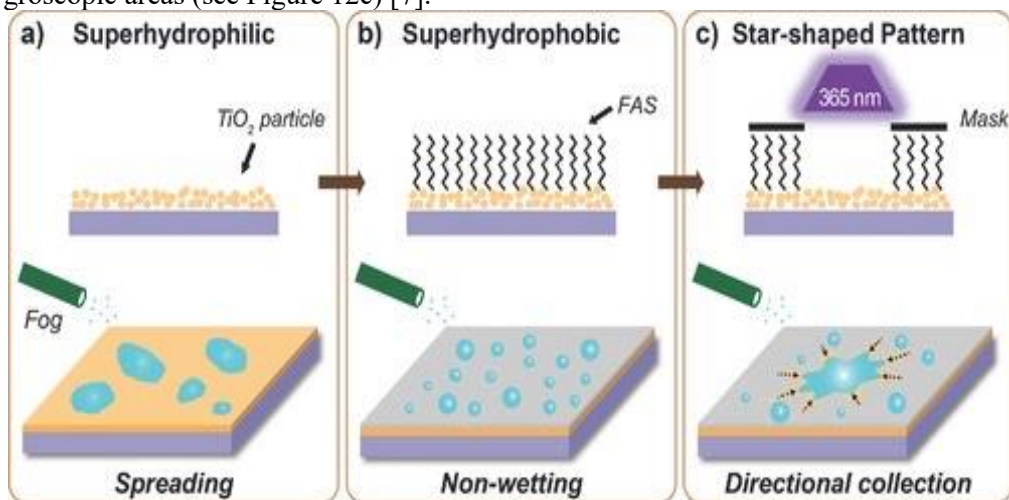


Figure 12. The procedure of making a star wettability pattern [7].

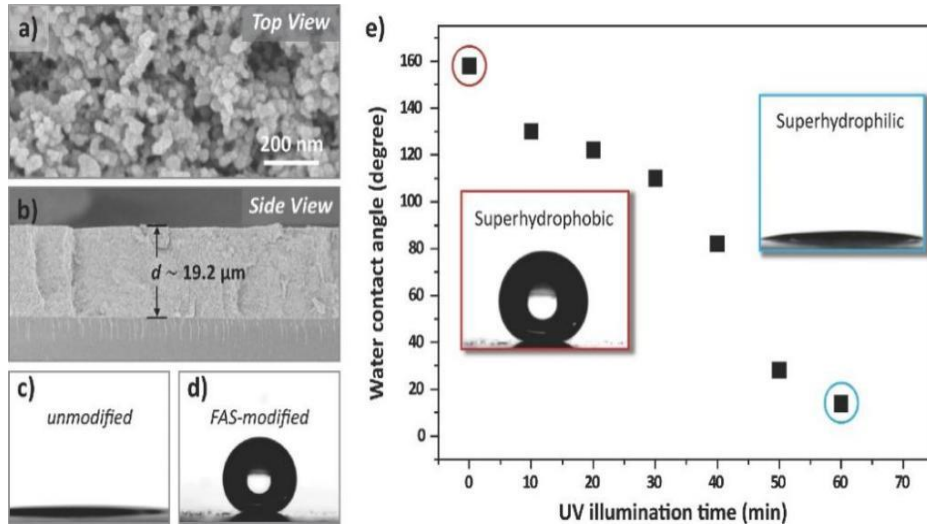


Figure 13. The properties of a patterned surface [7].

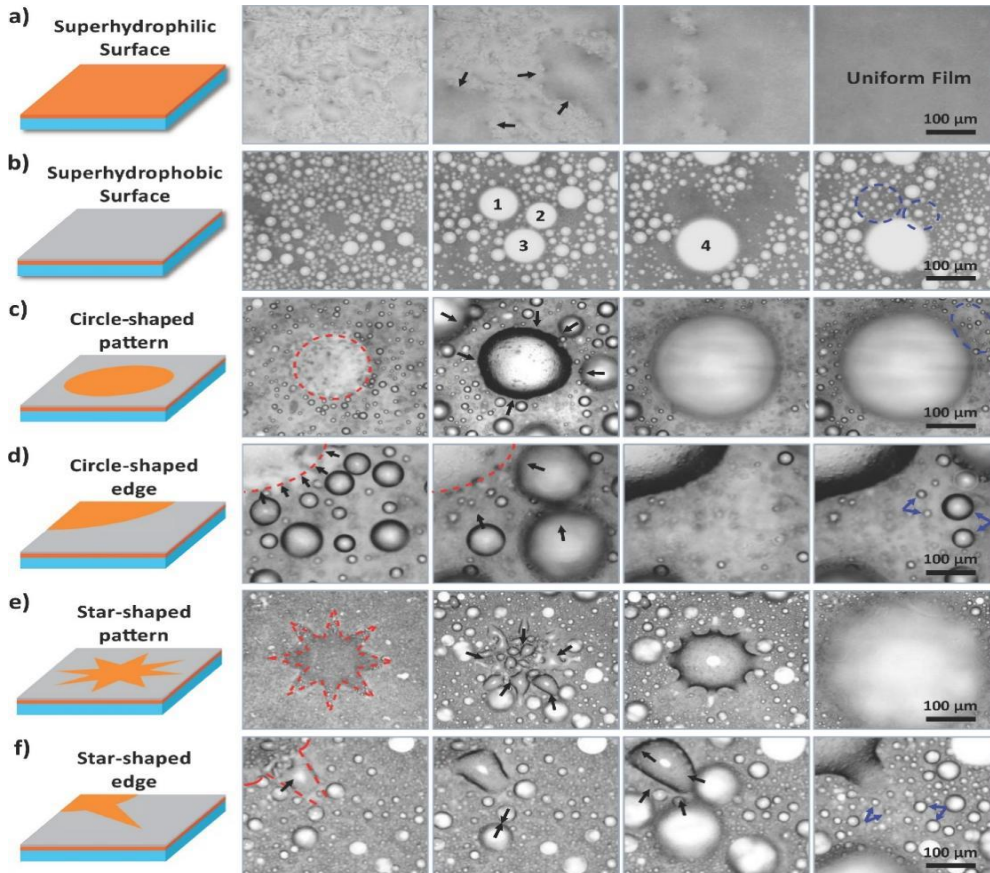


Figure 14. Different fog-collecting processes [7].

When a surface is homogeneously superhydrophilic, water drops scattered across it; when a surface is evenly superhydrophobic, individual droplets clump at random; and when a surface is bioinspired and has a pattern of hydrophilicity, small water droplets gather in one direction to the more wettable zone. [7]. Different fog-collecting processes will lead to different wettability features, which is shown in Figure 14.

Another example of patterned wettability surface is developed and called hybrid-patterned copper tubes. In order to improve the condensation heat transfer performance, the copper tubes are made into hydrophobic region β and less-hydrophobic region α to increase the condensate removal rate. Due to the hydrophobicity difference between region β and region α , a wettability gradient will be generated so that the condensate will mitigate, and the removal rates will be increased. Region β is served as droplet nucleation sites with rapid droplets mobility, while region α is served as drainage paths to promote droplets removal from region β due to the surface tension forces (see Figure 15).

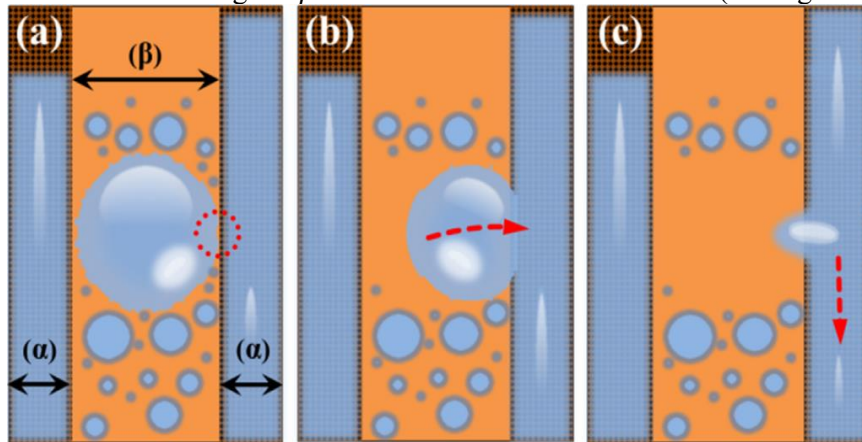


Figure 15. The principle of two distinct wettability areas [8].

(a) As condensed droplets develop in the β region and they will eventually contact the surrounding regions α . (b) The droplet(s) is dragged from the lower wettability area to the higher one (region β to region α) due to the interstitial fluid phenomenon, which is caused by the presence of two wettability adjacent regions. (c) Under the force of gravity, complete droplet removal and drainage take place in the greater wettability area [8].

The droplets prefer to form on the region α rather than on the region β at the start of condensation on a hybrid-patterned copper tube. The area will then be covered in a liquid coating as a result of the ongoing condensation, which will lower the temperature. It will be favored for droplets to develop due to the presence of the vapor in the area.

Figure 16 depicts the creation of a hybrid-patterned copper tube. After being polished, the copper tube's surface was washed with sulfuric acid, acetone, ethanol, and deionized water. The washed copper tube was dried with a nitrogen stream. The chosen straight stripes were then printed with black ink by using a laser printer on a standard sheet. The pellucid sheet was then evenly placed on top of the photoresist sheet with the printed side facing the photoresist sheet. The unexposed portions of the photoresist sheet retained its original rubbery state after being exposed to an UV ray source for 2–3 minutes, but the exposed portions of the photoresist sheet became fragile. The photoresist sheet was then precisely trimmed to a length that matched the copper tube's outer diameter and stretched around the tube with its adhesive side facing the tube's exterior. After that, within an abrasive blast cabinet, the tube was held and rotated by hand, and the blasted stream was applied by using a portable mini injector to aim orthogonally and about two to three inches from the surface of the container. The tube was then cleaned and dried once the mask had been taken off. After spending an hour at 70 degrees in a 0.0025 mol/L solution of n-Octadecyl Mercaptan and ethanol, the sample was rinsed and dried. [8].

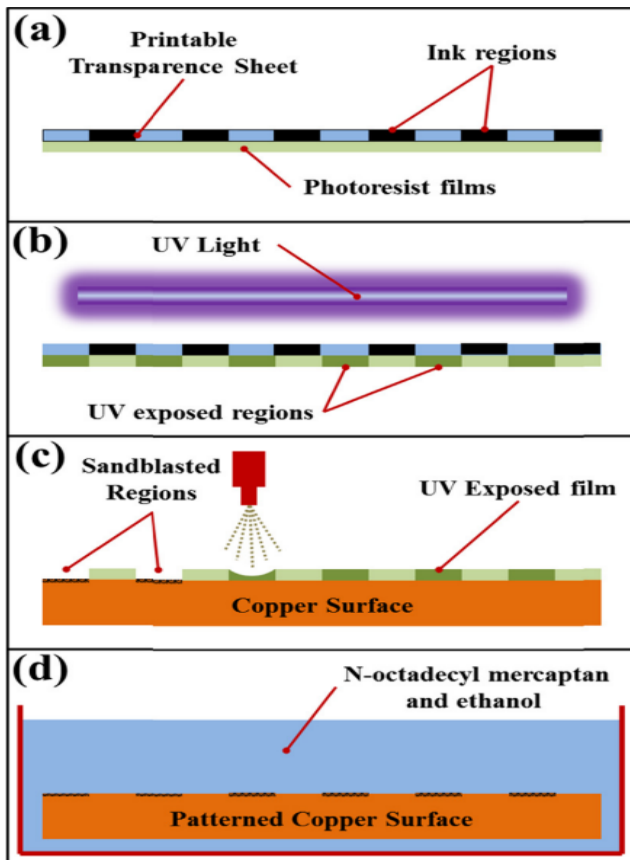


Figure 16. An illustration of the key steps in creating a composite wettability pattern on the condensing surface.

(a) Attaching the pellucid sheet with the intended pattern printed on it to the photoresist sheet. (b) Positioning both sheets in front of a UV light source with the pellucid sheet side facing out. Only the exposed portions of the photoresist film will become fragile and exactly match the engraved pattern on the pellucid sheet. (c) Thoroughly adhere the photoresist sheet to the condensate surface with the aid of the implant surface. When using a mini blasting procedure on the photoresist side, the tiny flow can only hit the contact area that is collecting underneath the fragile sections of the photoresist sheet. This enables the development of fragile areas that fit the photoresist sheet's pattern design. (d) After washing the condensing surface and removing the photoresist sheet residue, the condensed surface bearing the roughened pattern was submerged in the SAM solution for an hour [8]. To sum up, it is possible to regulate the flow direction of the atmospheric water droplets that are collected based on the analysis of surfaces with patterned wettability.

2.6. Filmwise and dropwise condensation

Condensation is a process of cooling the vapor to the liquid phase. It is widely used in water harvesting, industries, refrigeration, distillation columns, and power generation. Filmwise condensation (FWC) will take place if the fluid condenses fast, produces a thin layer, and covers the whole region with moisture. This may be seen on hydrophilic surfaces, which is caused by the condensing surface's high surface energy. On the other hand, if the liquid droplets form but the surfaces are not moist, DWC will occur. This may be seen on hydrophobic surfaces, which is caused by the condensation surface's low surface energy [9]. A constant liquid film is formed on the surface by filmwise condensation (FWC), whereas tiny droplets are formed by dropwise condensation (DWC) [10].

Condensation is a nucleation and growth phenomenon, which describes the formation of the expanding droplets. On hydrophilic surfaces, the nucleation rate is extremely high since the surfaces are favorable for molecules to nucleate on the surfaces. High nucleation rate will cause a high heat transfer coefficient (HTC). The heat transfer coefficient measures the amount of heat that may be transferred convectively between a fluid and the surface it flows over [11]. However, once the film is formed,

further nucleation will not happen, and the HTC will be dropped. The point of continuous liquid film formation is called the critical heat flux (CHF). Since the nucleation stops, the CHF will be low on hydrophilic surfaces. On the other hand, on hydrophobic surfaces, the nucleation rate is relatively low since the surfaces have a high Young's contact angle. A low nucleation rate will lead to a low HTC. However, since a continuous film will not be formed on hydrophobic surfaces, the CHF will be high. To sum up, hydrophilic surfaces have a larger HTC than hydrophobic surfaces, but hydrophilic surfaces have a smaller CHF than hydrophobic surfaces.

Condensation that occurs in films and drops is quite widespread in the industrial sector. Copper tubes are a common instance. After the smooth copper tube is treated with oxygen plasma, steam condensation will take place and create a continuous liquid coating (see Figure 17a). On the other hand, vapor condensation will happen and result in separate water droplets when the smooth copper tube is hydrophobized by a silane treatment (see Figure 17b). Condensate will infiltrate into the connecting pores of the porous silica inverse opals that are deposited on the copper tube (see Figure 17c). This is because the hydrophilic nature of the underlying substrate (silica-coated copper) and the silicon inverted mosaic structure. In addition to the coating's homogenous wettability brought on by the inverse opal coating's superhydrophilic nature, another biphilic surface - a hydrophilic base with repellent tips - is employed to link nucleating droplets via liquid bridges. When silane is used to chemically functionalize the inverse opal structure and silicone oil is used to permeate it, vapor condense will happen and highly mobile water droplets will develop that leave at a reduced length scale (see Figure 17d). This precipitation is known as SLIPS condensation, which can increase the rate of heat transfer by cutting the departure radius by almost 50% [12].

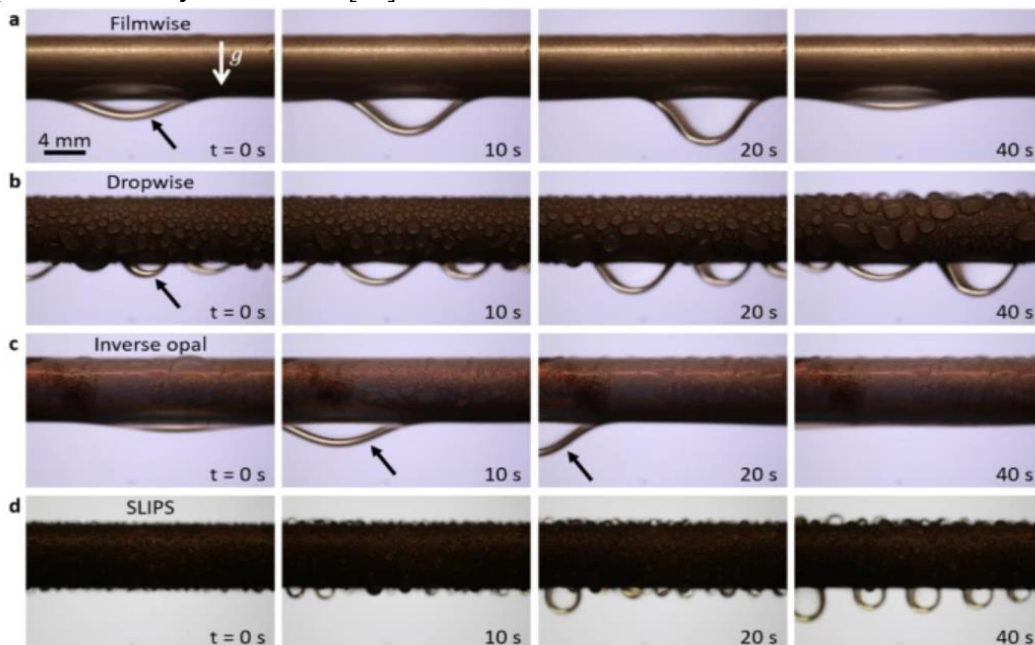


Figure 17. Pictures of water condensing on copper tubes with various surface treatments over time, demonstrating several condensation processes. (a) FWC on a smooth copper tube treated with plasma; (b) DWC on a flat hydrophobized copper tube; (c) IOC on a copper tube covered with silica inverse opal; (d) SLIPS precipitation on an oiled and porous surface.

Condensate was discharged vertically downward in all but IOC situations where gravity won out over anchoring forces. However, the condensation was carried through the fissures preferentially in an axial orientation during IOC. The condensate only migrated axially to the right or to the left, which is determined by the shape, size, and direction of the crack [12].

3. Natural surfaces and synthetic surfaces

3.1. Namib beetle

3.1.1. Properties of Namib beetle's wings. In nature, the surface of the Namib desert beetle's wings is an example of a hybrid hydrophilic and hydrophobic surface. Due to the extremely arid climate in the desert, water resources are scarce. The Namib beetle's wings enable them to collect water from the fog in the desert to survive. The Namib beetle's wings consist of waxy-coated hydrophobic regions and non-waxy-coated hydrophilic regions (see Figure 18).



Figure 18. The Namib desert beetle's hybrid wings [13].

The presence of hydrophilic regions makes it easy to absorb water fog from the wind, that is, the vapor will easily condense in the hydrophilic regions. The presence of hydrophobic regions enables the water droplets to roll down to the beetle's mouth. To achieve water harvesting, the Namib beetles will set their wings back towards the direction of the wind so that the moisture in the air by way of condensation of water vapor can condense into bulge parts to form water droplets. Then, the water droplets will keep increasing gradually, after the droplets reach the critical value, they will quickly slip to drain at the bottom of the grooves, and along with the bow back tumble into the mouth.

3.1.2. Synthesis of hybrid hydrophilic and hydrophobic surface. The function of the Namib desert beetle's wings is used for fog harvesting. The arrangement of hydrophilic bulges and hydrophobic bases plays a significant role in water harvesting. On the other hand, if the texture is entirely hydrophilic, the water will not slide or roll down but forms a layer of water; if the texture is entirely hydrophobic, the water will not roll down towards the mouth of the beetle specifically but be blown away by the wind or the sand waves. The pulsed laser deposition (PLD) [14] method is developed for the synthesis of the texture with hybrid hydrophilic and hydrophobic surfaces, which is versatile and effective for condensing water. PLD is able to assist the growth of the films by transferring the stoichiometric energies, energetic beam, etc [15]. To make a hybrid hydrophilic and hydrophobic surface (see Figure 19), the original hydrophilic texture was sprayed with the silica polydimethylsiloxane PDMS to create a hydrophobic coating on its surface. Then platinum was used as another coating by using the above PLD method and stainless steel was meshed as masks. Afterward, the desired beetle-inspired surface would be formed, whereas the hydrophilic, and the white areas are hydrophobic.

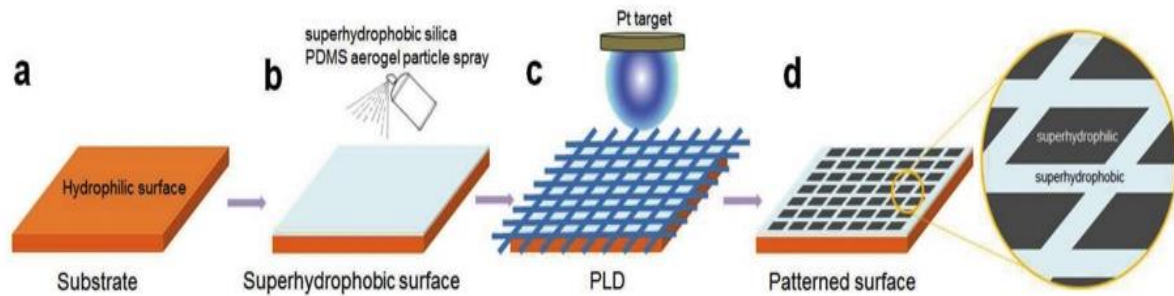


Figure 19. The diagram of the synthesis of a hybrid hydrophilic and hydrophobic surface by using the PLD method [16].

Compared with the textures that are only applied with PDMS or Pt coating, the combination of the two coatings technically creates the patterned arrangements of the two features instead of solely hydrophilic or hydrophobic, which is more desirable for the water condensation. The patterned synthetic surface could reach the effectiveness of liquid condensing up to $5300 \text{ mg/cm}^2\text{h}^{-1}$ [14].

3.2. Butterfly wings

3.2.1. Properties of butterfly wings. An example of a naturally occurring superhydrophobic surface is the surface of butterfly wings. When the contact angles of various butterfly wings were measured, it was discovered that they were all greater than 150 degrees. The Cassie-Baxter state results from the placement of water droplets on the wings. Their wings have a special characteristic that ensures the water droplets will only move in the radical outward (RO) direction of the body's central axis (see Figure 20). The feature of butterfly wings can be visualized after zooming in, which is shown in Figure 21.

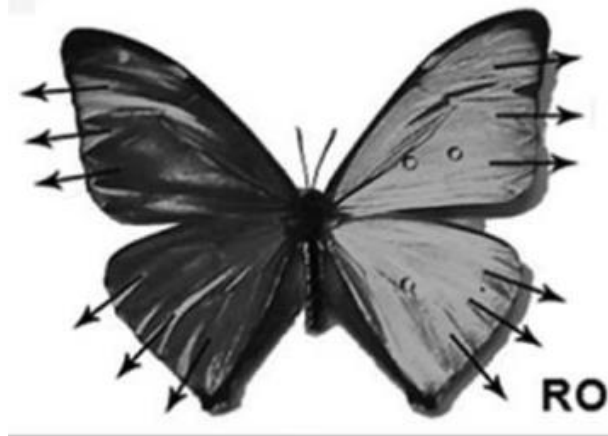


Figure 20. The diagram of the radical outward (RO) direction of the butterfly wings [17].

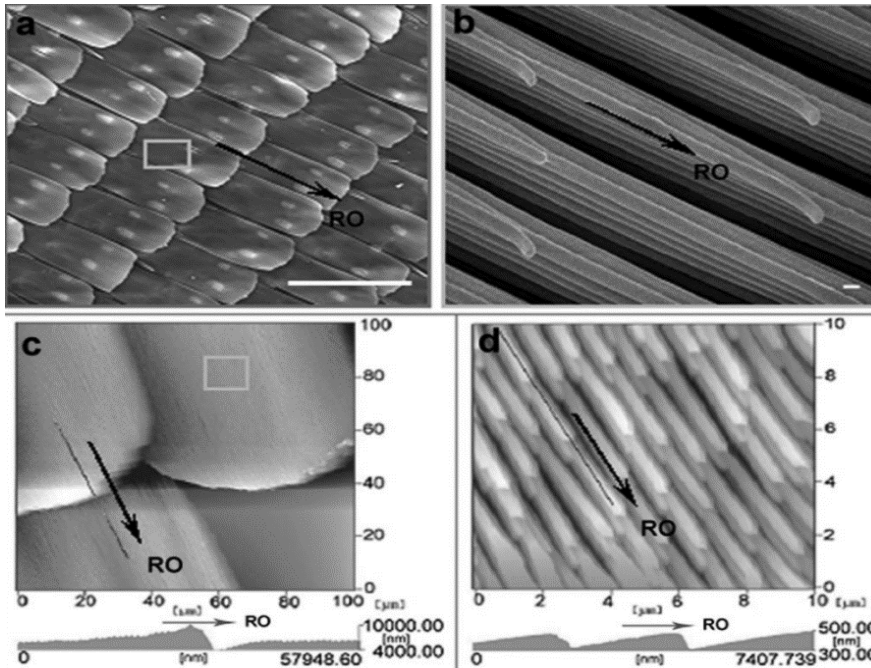


Figure 21. (a, b) The periodic arrangement of overlapping microscales on the wings and tiny lamella-stacking nanostripes on the scales can be seen in the SEM pictures. (c,d) The overlapping micro-scale and nano-stripe patterns as shown in the AFM photos [17].

Hierarchical micro- and nanostructures were discovered on the surface of a butterfly wing by using a JEOL JSM-6700F field-emission scanning electron microscope (FE-SEM) operating at 3 kV. Atomic force microscopy (AFM) in the tapping mode was used to determine the wing's three-dimensional topologies and cross-sections [17]. The hierarchical feature enabled the water droplets to slip easily. When the wings are tilted downward, the water droplets will roll along the RO direction easily. On the other hand, when the wings are tilted upward, the water droplets will be pinned on the wings but not roll along the opposite direction to the RO direction, which is called the directional adhesion (see Figure 22).

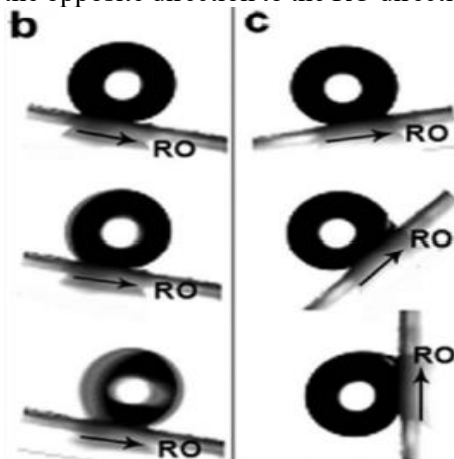


Figure 22. Wings of a butterfly with extreme hydrophobicity. (b) When the wing is inclined below by 90° , the droplet rolls along the RO direction easily. (c) Even when the wing is fully vertical, the droplet is firmly fixed on it [17].

3.2.2. Manipulating water droplets by anisotropic surface. A nanoindentation gadget featuring integrated vertices in double different superwettability tracks (IMDDS) is created based on the wettability of the butterfly wings. IMDDS can rationally rotate a layer of superhydrophilic rail and a layer of superhydrophobic rail to dynamically modify the overall surface wettability and further adjust the anchoring and sliding of the droplets.

Copper wires can be used to build the IMDDS gadget. Figure 23 shows the technology for copper wires with various super-wettabilities. By washing with ethanol, acetone, deionized water, and 0.1 M HCl for 20 min, superhydrophilic (SHL) copper wires were produced, which were subsequently dried in nitrogen. Copper wires were then submerged for three minutes in an aqueous solution made by combining 2 g of NaOH, 0.86 g of $(\text{NH}_4)_2\text{S}_2\text{O}_8$, and 34.4 g of water. Then, copper wires were treated

with silicone oil (0.3 g) diluted with n-octane (3.2 g) for 48 hours to produce superhydrophobic (SHB) copper wires.

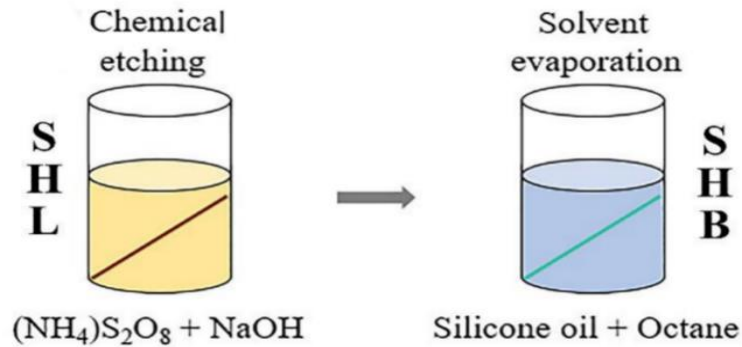


Figure 23. Blueprints of the production of various superwettability copper wires. Because of being corroded, the copper string's surface is superhydrophilic (SHL), then after being submerged in silicone oil, it becomes superhydrophobic (SHB) [18].

After the processing of the copper wires was complete, the tubes of various sizes were coated with copper wires, and the inner layer (tube I) was placed into the outer tube (tube O). Figure 24 shows IMDDS.

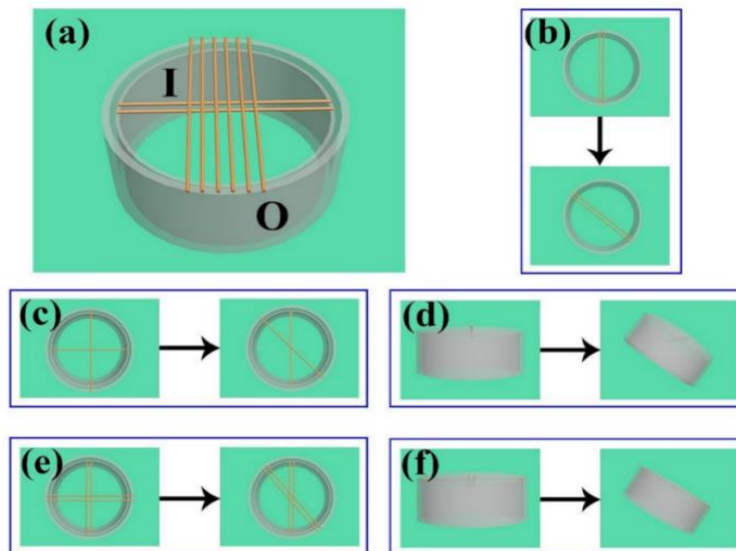


Figure 24. IMDDS and where it is located.

(a) The configuration of the IMDDS, which includes several wettable wires, an internal tube (tube I), and an external tube (tube O). (b) Modifying the inclination of one layer of wire to determine the droplet's velocity. To evaluate the PV of a water droplet, adjust the cross angle of the single wire (c) and double copper cabling (e) (the tube is vertical). By adjusting the tube's tilt angle, incorporating the single wire crucifix (d) as well as double wires cross (f), the droplet PV can be measured [18].

By turning the copper wires, the water droplets can slide and pin on the wires. The droplets can be regulated by adjusting the distance between two copper wires. Ultimately, IMDDS presents a new approach for the regulation of minute droplets and offers the probability for vast manufacturing and modification of the controller. IMDDS can precisely and simply modify the droplet orientation at any moment without relying on external energy [18].

3.3. Spider web

3.3.1. *Theoretical basis of water collection of spider silk materials.* A structure of mixed hydrophilicity and hydrophobicity can also be seen in spider web. Spider textiles are capable of collecting water in various ways. Spider-capture-silk (SCS) features distinctive recurring spinning knots that are either covered with glycosyl droplets or comprised of randomly dispersed nanofibrils. Condensation and directed collecting of water droplets from the atmosphere can be achieved by SCS's special feature (see Figure 25).

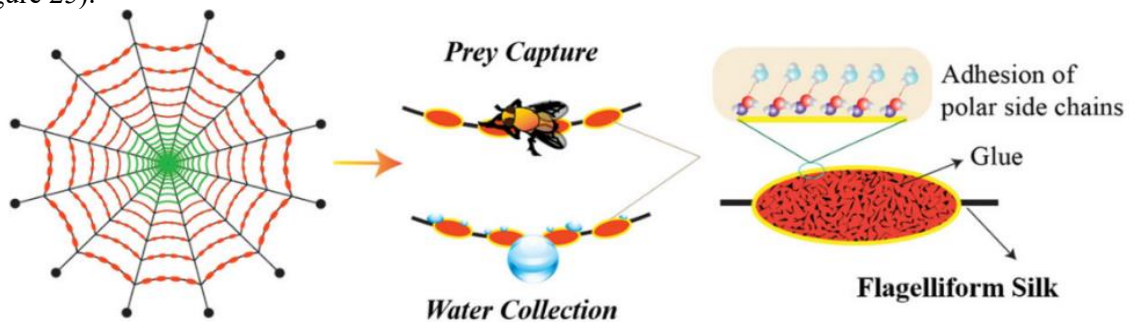


Figure 25. The arrangement, basis, and surface of SCS [19].

The tiny liquid droplets that are concentrated distilled water and aggregate to create bigger droplets attributed to the variations in Laplace pressure and surface energy gradient between nodes and joints.

Spider webs also have the elasticity to stabilize under a variety of circumstances, including the impact of prey, harsh weather, and falling debris. When outside pressures are applied to the web, the hydrogen bonding of protein chains will be rearranged. This will result the silk in the rise of molecular orientation and internal free energy with low entropy. In addition, the supercontraction in the fiber brought on by the condensate captured from environment will cause the protein chains to rotate to lower energy with a high entropy. Because of this cyclical mechanism, the web may adapt to humid and reverse distortion and degeneration (see Figure 26) [19].

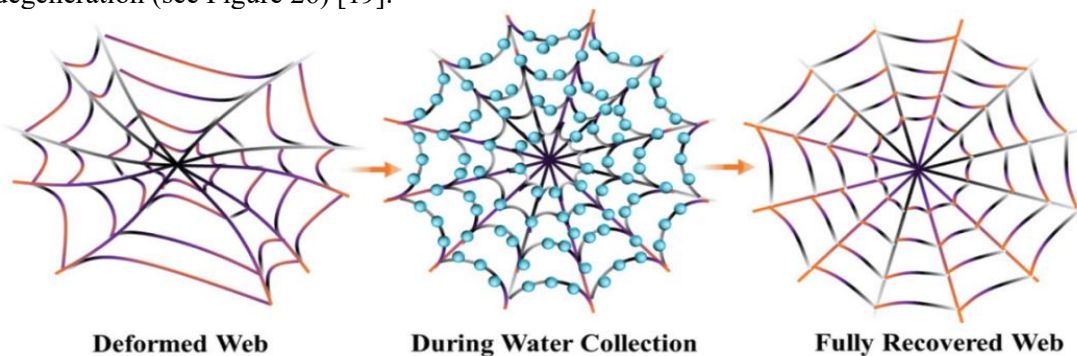


Figure 26. Spider webs feedback to alternating environmental circumstances [19].

In 2010, Zheng et al [20] investigated the water absorption of the silk of the crustacean spider *Uloborus Walckenaerius*. SEM pictures of the silk structure under dry circumstances and in fog change into regular spinning connections (see Figures 27). The unusual fiber structure of the capture filament, which consists of periodical spin junctions constructed of random nanofibers that are aligned after being soaked in water, is said to be the reason of its moisture capacity. Based on the structural properties, it leads to the difference of Laplacian pressure and the surface energy imbalance between spindle connection and the joint. Consequently, an interfacial gradient and a Laplace pressure difference lead to the continuous humidity and dimensional collection of submillimeter-sized droplets around the axle interface, but the motion of micrometer droplets appears more challenging when neither of these forces alone can conquer the significantly bigger latency impact. Spider silk demonstrates its directional water collecting capabilities through the combined action of these two elements [20].

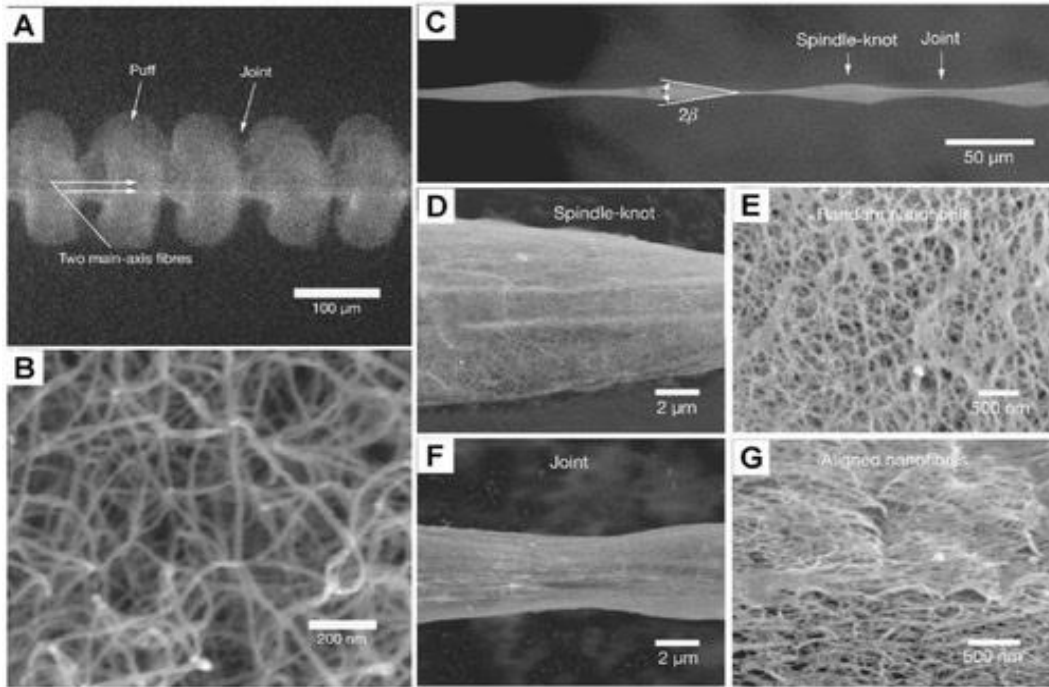


Figure 27. *Uloborus walckenaerius*, a crustacean spider's structure.

Two spindle fibers are seen in (A) a low magnification environmental scanning electron microscopy (SEM) picture that is framed by recurring puffing and connections. (B) The puffs' enlarged picture shows many nanoparticles. Images are captured by using an environmental scanning electron microscope (C) to show thin joints joined by cyclical spindle joints. Illustration of the spindle junction magnified in (D). Image of a spindle junction magnified (E). Low joint magnification (F). Images of joints at higher resolution (G) show nanofibers that are essentially parallel to the filament axis [20].

Observation under the scanning electron microscope showed that single spider silk appeared as a special periodic spindle fiber after being wet. The morphology and structure can also be approximately described as a bead string fiber; this structure can produce the Laplace pressure difference and the surface energy gradient exert a driving force on the droplet on the fiber to move it toward the center of the spindle segment. These driving forces help droplets transport and merge into large droplets so that they will fall and be collected due to gravity, which will also achieve high-efficiency fog harvesting. As shown in Figure 28a, the droplet is driven by the Laplace force (FL) on the tapered structure, which can be expressed by the following equations [21-24]:

$$F_L = \gamma \left(\frac{1}{R_{1'}} - \frac{1}{R_{2'}} \right) \frac{\sin \beta}{R_1 - R_2} V \quad (7)$$

Where γ is the surface tension of the droplet, $R_{1'}$ and $R_{2'}$ are the local curvature of the three-phase contact line at both ends of the droplet along with the spindle node, respectively, R_1 and R_2 are the radius of curvature at both ends of the local spindle node. β is the semi-apex Angle of the spindle node and is related to the shape and size of the spindle node. V is the volume of the droplet at the spindle node. Since spindles of spider silk have higher axial roughness than fiber segments, spindles of spider silk are more hydrophilic and have higher surface energy, so that the contact angle between spindles and water will be smaller.

The driving force of droplet on the structure with wettability gradient or surface energy gradient (see Figure 28b) can be calculated by the following equation [23,25]:

$$F_S = \int_{L_1}^{L_2} \gamma (\cos \theta_1 - \cos \theta_2) dl \quad (8)$$

Where θ_1 and θ_2 respectively represent the contact angle of the droplet at different two points on the spider silk, dl is the integral variable from the fiber segment (L_1) to the spindle segment (L_2). In addition, there are pores on the spider silk fiber that can absorb water, and the spindles of spider silk-like materials can also be prepared into porous, groove, spiral and other structures. These structures assist the water harvesting process through capillary forces (see Figure 28c), which can be expressed as follows:

$$C = \frac{2\gamma}{R'} \quad (9)$$

Where, C is the capillary force on the droplet; R' is the radius of curvature of the droplet in the capillary (i.e. the pore or groove on the surface of the material), and is related to the contact angle and capillary thickness.

Compared with single bionic spider silk, the water collection performance of the water collection material imitating desert beetle and cactus is lower per unit volume or mass. However, since the material itself is a planar or three-dimensional material, it has a large scale and is technically easier to achieve scale-up preparation. At present, the material exhibits a large scale of water collection. Since 2016, several studies [24, 26-28] have pointed out that a large number of intersecting structural units in topological spider webs can generate a driving force, which can be further deduced from Formula (7) or (8). This force tends to converge droplets towards the intersection, which has beneficial effects on droplet directional transport and final collection to improve the water collection efficiency. This has laid a foundation for the design of 2-D and 3-D cobweb multi-cross water harvesting materials in recent three years to expand the scale of water harvesting and realize industrial-scale water harvesting.

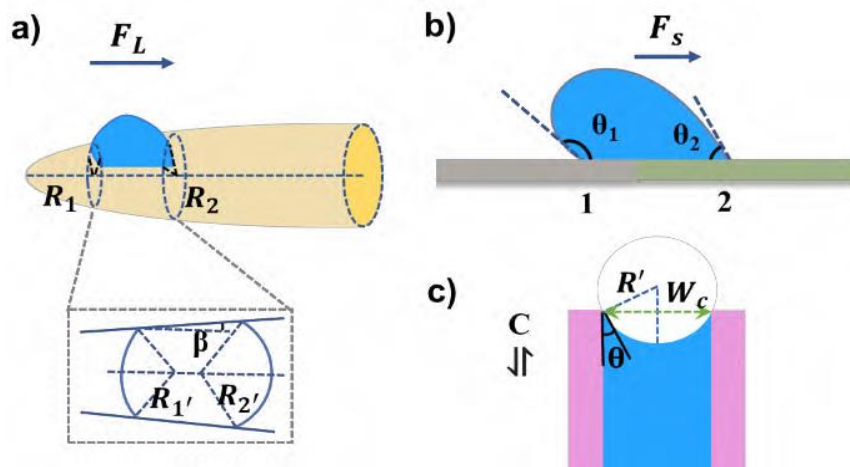


Figure 28. Force analysis sketch of droplets on bio-inspired fog-harvesting units [29].

3.3.2. Development of preparation technology of spider silk-like micro - nano composites. There are several methods when the intention is to obtain the spindle node or bead fiber and the corresponding water collecting function, including the dip-coating method, the electrodynamic method, fluid coating method, microfluidics. These methods can use various types of raw materials to prepare micro-nano composite materials, including polymers, carbon materials, metal materials, biological materials, etc. In the last 3 years, the latest research uses machinery, textile, and other fields of technology to manufacture imitation spider web large-scale water collection materials.

3.3.3. Dip-coating. The horizontal immersion-lift method (lift method for short) is the earliest method used to prepare spider-like silk fibers (see Figure 29). First, the diameter of about 7-400 μm fibers (such as nylon, carbon fiber, copper wire, glass fiber, etc.) is deeply immersed in a pre-configured polymer solution. Then, it is pulled out of the polymer solution at a certain rate. At this point, the polymer solution will wrap around the fiber to form a film. Due to the principle of Rayleigh instability [24,30-32], thin

films are prone to rupture. Finally, the film breaks into many elliptic balls on the fibers, which are separated by the polymer solution phase through an evaporation process and eventually form periodic spindle node fibers or bead fibers. Based on the evaporation process, several technologies have been developed, such as sol-gel technology and the breath figure method [33-35]. Under a certain humidity environment, breaking thin films can produce porous and rough structures on the surface of the spindle node [36]. Since the lifting method is very simple, it has been further combined with spraying operation on the commercial road to achieve large-scale preparation.



Figure 29. Diagrammatic sketch of horizontal immersion-lift method [29].

3.3.4. Coaxial electrostatic spinning. Coaxial electrospinning is a combination of coaxial electrospinning and traditional electrospinning [37,38]. The bead fibers with diameter (200 nm~12 μ m) and relatively large nodes (3~6 times of fiber diameter) were easily prepared by this method. As shown in Figure 30, two-phase fluids with different vapor pressures and viscosity are sprayed through two different channels. The solution with lower concentration is sprayed as micron particles in the outer channel, forming a spindle or ellipsoid node. The fluid with higher viscosity in the inner channel is electrospun into micron or nano fibers [39]. This method was first used in other fields to prepare string fibers. After the spider silk water collecting mechanism was discovered, it was developed to prepare water collecting materials. This method can also be combined with breath-mapping, sol-gel, self-assembly and other processes, such as wet assembly electrospinning [40,41]. In most cases, the fibers prepared by electrospinning lack mechanical strength. However, in the last five years, they are also used to prepare films on the substrate of water collecting materials to strengthen water-collecting related functions [42,43]. In addition, biological materials or biocompatible materials can be used for spinning, liquid transfer, or microdroplet manipulation for medical purposes, such as drug release [44,45].

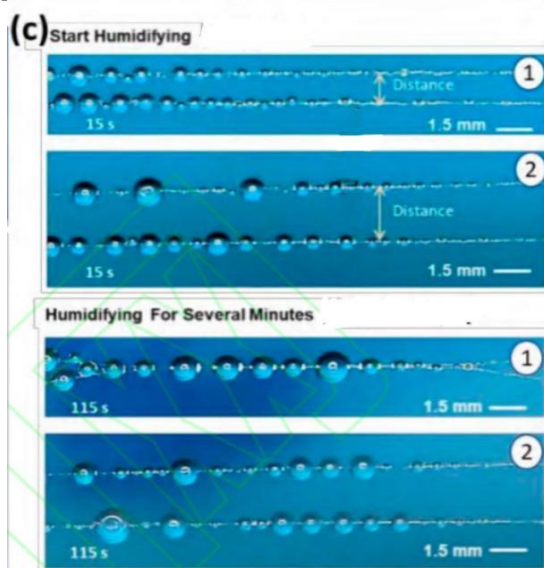


Figure 30. The coalescence behavior of droplet on parallel silk of spider web prepared by microfluidic method [46].

4. Conclusion

The majority of superhydrophobic surfaces have poor mechanical wear resilience and long-term endurance, which has limited their use in commercial or industrial applications [47]. The topography is unstable at the nanoscale, particularly for polymers. The instability makes them simply wind and dull down, which will eliminate their superhydrophobic qualities. The endurance of superhydrophobic surfaces is constrained because it is challenging to connect any superhydrophobic nanoparticle without damaging or deteriorating its superhydrophobic nature [48].

Another critical issue is coating lifetime. A given covering is said to last between 2 and 8 months in direct sunlight and outdoor circumstances, and up to one year or more for indoor applications and outside shielded [49]. Additionally, a coating can be removed by straightforward scratching or highly intense water steam. Although surfaces repel water, water vapor is not repelled. Condensation will occur if the coating's temperature is below the dew point, which will cause the surface to become wet and lose its superhydrophobic characteristic [48]. Because the coating lifetime is relatively short and easy to be washed off, it is necessary to keep renewing the coating surfaces. In return, the costs of superhydrophobic coating will increase. The average cost of superhydrophobic coating is around \$70 per 0.95 liters [49]. Besides coating, most of the fabrication methods require expensive processes. In addition, the majority of techniques (for example – lithography) are designed for tiny scales, therefore it is impossible to create vast area substrates with nanostructured surfaces by using the template approach. The price of making tiny chip dies and sewing them will rise considerably [48].

Furthermore, the majority of superhydrophobic coverings contain fluorine. High amounts of fluorine-based artifacts can impair kidneys, muscles, nerves, eyes, and nasal irritations in addition to causing major health problems such tooth and bone deterioration. Since the composition of coatings are inorganic compounds and polymers, which are non-biodegradable, the jettison of coatings will lead to potential environmental pollution [48]. Superhydrophobic surfaces are useful in many fields, especially critical in fog harvesting. However, the durability of superhydrophobic surfaces needs to be improved. In future studies, the use of materials and the efficiency of fog harvesting need to be focused.

Acknowledgment

Xinhui Song and Qijia Zhou contributed equally to this work and should be considered co-first authors, Bochao Cai and Ziyi Qiu contributed equally to this work and should be considered co-second authors.

References

- [1] Dehumidifier market size: Industry report, 2021-2028. Dehumidifier Market Size | Industry Report, 2021-2028. (n.d.). Retrieved March 29, 2022, from <https://www.grandviewresearch.com/industry-analysis/dehumidifier-market>
- [2] Stuart, J., LearnMetrics, Mike, Anni, Andrew, Hitech, & Nadim. (2021, August 12). Dehumidifier Power Efficiency: Do dehumidifiers use a lot of electricity? LearnMetrics. Retrieved March 29, 2022, from <https://learnmetrics.com/dehumidifier-energy-efficiency/>
- [3] By. (2022, February 18). How much does it cost to run a dehumidifier? (\$, W, kwh, time). LearnMetrics. Retrieved March 29, 2022, from <https://learnmetrics.com/cost-of-running-a-dehumidifier/>
- [4] Investigation of carbon fiber composite surface preparation processes for making unshakeable bonds. Ruckus Composites. (2021, June 18). Retrieved April 6, 2022, from <https://ruckuscomp.com/news/ruckus-labs/2021/06/18/surface-energy-study/>
- [5] Contact Angle Hysteresis explained. ACS Publications. (n.d.). Retrieved March 30, 2022, from <https://pubs.acs.org/doi/10.1021/la060254j>
- [6] Tuteja A, Choi W, Ma M, Mabry JM, Mazzella SA, Rutledge GC, McKinley GH, Cohen RE. Designing superoleophobic surfaces. *Science*. 2007 Dec 7;318(5856):1618-22. doi: 10.1126/science.1148326. PMID: 18063796.
- [7] Bai H;Wang L;Ju J;Sun R;Zheng Y;Jiang L; (n.d.). Efficient Water Collection on integrative bioinspired surfaces with star-shaped wettability patterns. *Advanced materials* (Deerfield

- Beach, Fla.). Retrieved April 2, 2022, from <https://pubmed.ncbi.nlm.nih.gov/24847736/>
- [8] Alwazzan, M., Egab, K., Peng, B., Khan, J., & Li, C. (2017, May 19). Condensation on hybrid-patterned copper tubes (i): Characterization of condensation heat transfer. *International Journal of Heat and Mass Transfer*. Retrieved April 12, 2022, from <https://www.sciencedirect.com/science/article/pii/S0017931016339394#:~:text=The%20results%20reveal%20that%20all,with%20a%20complete%20dropwise%20condensation.>
- [9] Chatterjee, A., Derby, M. M., Peles, Y., & Jensen, M. K. (2013, August 23). Condensation heat transfer on patterned surfaces. *International Journal of Heat and Mass Transfer*. Retrieved April 1, 2022, from <https://www.sciencedirect.com/science/article/pii/S0017931013006315>
- [10] Hu, X., Yi, Q., Kong, X., & Wang, J. (2021, February 9). A review of research on Dropwise Condensation Heat Transfer. MDPI. Retrieved April 1, 2022, from <https://www.mdpi.com/2076-3417/11/4/1553>
- [11] Kurganov, V. A. (n.d.). Heat transfer coefficient. THERMOPEDIA. Retrieved April 1, 2022, from <https://www.thermopedia.com/content/841>
- [12] Adera, S., Naworski, L., Davitt, A. et al. Enhanced condensation heat transfer using porous silica inverse opal coatings on copper tubes. *Sci Rep* 11, 10675 (2021). <https://doi.org/10.1038/s41598-021-90015-x>
- [13] Attinger, D., Frankiewicz, C., Betz, A., Schutzius, T., Ganguly, R., Das, A., . . . Megaridis, C. (2014). Surface engineering for phase change heat transfer: A review. *MRS Energy & Sustainability*, 1, E4. doi:10.1557/mre.2014.
- [14] Yu, Zhenwei et al. Desert Beetle-Inspired Superwetable Patterned Surfaces For Water Harvesting. 2017.
- [15] Lowndes, Douglas H. et al. Synthesis Of Novel Thin-Film Materials By Pulsed Laser Deposition. 1996.
- [16] Parker, Andrew R., and Chris R. Lawrence. Water Capture By A Desert Beetle. 2001.
- [17] Zheng, Y., Gao, X., & Jiang, L. (2007). Directional adhesion of superhydrophobic butterfly wings. *Soft Matter*, 3(2), 178-182.
- [18] Liang, X., & Guo, Z. (2020). Mechano-adjusted anisotropic surface for manipulating water droplets. *Chemical Engineering Journal*, 395, 125110.
- [19] Venkatesan, H., Chen, J., Liu, H., Liu, W., & Hu, J. (2020). A Spider-Capture-Silk-Like Fiber with Extremely High-Volume Directional Water Collection. *Advanced Functional Materials*, 30(30), 2002437.
- [20] Zheng Yongmei, Bai Hao, Huang Zhongbing, et al. Directional water collection on wetted spider silk[J]. *Nature*, 2010Y, 463:640 - 643.
- [21] Ju J, Bai H, Zheng Y, et al. A multi-structural and multi-functional integrated fog collection system in cactus[J]. *Nat Commun*, 2012, 3: 1247
- [22] Zhou H, Zhang M X, Li C, et al. Excellent Fog-Droplets Collector via Integrative Janus Membrane and Conical Spine with Micro/Nanostructures[J]. *Small*, 2018, 14: 1801335
- [23] Zheng Y M, Bai H, Huang Z B, et al. Directional water collection on wetted spider silk[J]. *Nature*, 2010, 463: 640-643
- [24] Li C, Liu Y F, Gao C L, et al. Fog harvesting of a bioinspired nanocone-decorated 3D fiber network[J]. *ACS Appl Mater Interfaces*, 2019, 11: 4507-4513
- [25] Xu C X, Jia Z H, Lian X H, et al. Wetting and adhesion energy of droplets on wettability gradient surfaces[J]. *J Mater Sci*, 2020, 55: 8185-8198 Tian Y, Zhu P A, Tang X, et al. Large-scale water collection of bioinspired cavity microfibers[J]. *Nat Commun*, 2017, 8: 1080
- [26] Dong H, Zheng Y, Wang N, et al. Highly efficient fog collection unit by integrating artificial spider silks[J]. *Adv Mater Interfaces*, 2016, 3: 1500831
- [27] Tian Y, Zhu P A, Tang X, et al. Large-scale water collection of bioinspired cavity microfibers[J]. *Nat Commun*, 2017, 8: 1080
- [28] Dong H, Zheng Y, Wang N, et al. Highly efficient fog collection unit by integrating artificial spider silks[J]. *Adv Mater Interfaces*, 2016, 3: 1500831

- [29] Li C, Ni Z. Water collection performance of biomimetic spider silk micro / nano composites Journal of composite materials doi:10.13801/j.cnki. fhclxb. 20220107.001.
- [30] Xue Y, Chen Y, Wang T, et al. Directional size-triggered micro- droplet target transport on gradient-step fibers[J]. J Mater Chem A, 2014, 2: 7156-7160
- [31] Quéré D, Meglio J M D, Brochard-Wyart F. Spreading of liquids on highly curved surfaces[J]. Science, 1990, 249: 1256-1260
- [32] Song J N, Zhang W L, Wang D H, et al. Polymeric microparticles generated via confinement-free fluid instability[J]. Adv Mater, 2021, 33: 2007154
- [33] Tang M, Christie K S S, Hou D Y, et al. Fabrication of a novel un- derwater- superoleophobic/hydrophobic composite membrane for robust anti-oil-fouling membrane distillation by the facile breath figures tem- plating method[J]. J Membr Sci, 2021, 617: 118666
- [34] Huang J J, Hao H Y, Huang Y. Gradient porous structure templated by breath figure method[J]. Langmuir, 2021, 19: 6016-6021
- [35] Cheng R M, Colombo R N P, Zhang L. et al. Porous Graphene Oxide Films Prepared via the Breath-Figure Method: A Simple Strategy for Switching Access of Redox Species to an Electrode Surface[J]. ACS Appl Mater Interfaces, 2020, 11: 55181-55188
- [36] Feng S L, Hou Y P, Chen Y, et al. Water-assisted fabrication of po- rous bead-on-string fibers[J]. J Mater Chem A, 2013, 1: 8363-8366
- [37] Loscertales I G, Barrero A, Guerrero I, et al. Micro/nano encapsulation via electrified coaxial liquid jets[J]. Science, 2002, 1695: 295
- [38] Sun Z C, Zussman E, Yarin A L, et al. Compound core-shell polymer nanofibers by co- electrospinning[J]. Adv Mater, 2003, 15: 1929
- [39] Zhang M X, Zheng Y M. Bioinspired structure materials to contro water-collecting properties[J]. Materials Today-Proceedings, 2016, 3: 696-702
- [40] Zhao L, Song C, Zhang M X, et al. Bioinspired heterostructured bead-on-string fibers via controlling the wet-assembly of nanoparticles[J]. Chem Comm, 2014, 50: 10651-10654
- [41] Song C, Zhao L, Zhou W B, et al. Bioinspired wet-assembly fibers: from nanofragments to microhumps on string in mist[J]. J Mater Chem A, 2014, 2: 9465-9468
- [42] Ren B N, Pi H H, Zhao X, et al. Janus membrane with novel directional water transport capacity for efficient atmospheric water capture[J]. Nanoscale, 2021 13: 9354-9363
- [43] Zhang Y P, Yang J H, Li L L, et al. Facile fabrication of superhydrophobic copper-foam and electrospinning polystyrene fiber for combinational oil-water separation[J]. Polymers, 2019, 11: 97
- [44] Kanu N J, Gupta E, Vales, U K, et al. Electrospinning process parameters optimization for biofunctional curcumin/gelatin nanofibers[J]. Mater Res Express, 2020, 7: 035022
- [45] Zhang P W, da-Silva G M, Deatherage C, et al. Cell-penetrating peptide mediates intracellular membrane passage of human papillomavirus L2 protein to trigger retrograde trafficking[J]. Cell, 176: 1465
- [46] Liu Y F, Yang N, Li X, et al. Water harvesting of bioinspired microfibers with rough spindle-knots from microfluidics[J]. Small, 2020, 16: 1901819
- [47] Milionis, A., Loth, E., & Bayer, I. S. (2016). Recent advances in the mechanical durability of superhydrophobic materials. Advances in colloid and interface science, 229, 57-79.
- [48] Manoharan, K., & Bhattacharya, S. (2019). Superhydrophobic surfaces review: Functional application, fabrication techniques and limitations. Journal of Micromanufacturing, 2(1), 59-78.
- [49] MacKenzie, A. (2015, May 2). Ultra-ever dry hydrophobic coating repels almost any liquid. New Atlas. Retrieved April 19, 2022, from <https://newatlas.com/hydrophobic-coating-repels-liquids/26286/>